Supplementary Information

# Controlling the alignment of 1D nanochannel arrays in oriented metal-organic framework films for host-guest materials design

Kenji Okada,[a, b]* Miharu Nakanishi,[a] Ken Ikigaki,[a] Yasuaki Tokudome,[a] Paolo Falcaro,[c] Christian Doonan[d] and Masahide Takahashi[a]*

[1] *Department of Materials Science, Graduate School of Engineering, Osaka Prefecture University, Sakai, Osaka, 599–8531, Japan.* [2] *JST, PRESTO, 4-1-8 Honcho, Kawaguchi, Saitama, 332-0012, Japan.* [3] *Institute of Physical and Theoretical Chemistry, Graz University of Technology, Stremayrgasse 9, Graz 8010, Austria.* [4] *Department of Chemistry, The University of Adelaide, Adelaide, South Australia 5005, Australia*
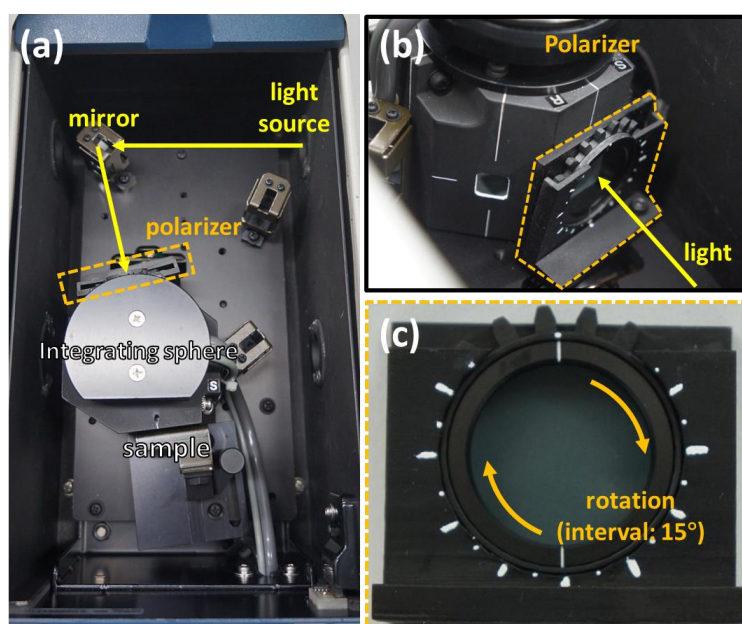
**Figure S1.** The experimental setup for the polarization-dependent UV/Vis measurements. Photos of a sample chamber in UV/Vis spectroscopy machine (a) and the polarizer (b-c), where the light path is shown in yellow arrow. The incident light is polarized at the input port of integrating sphere with interval angle, 15°. The polarization dependence of light absorption was measured for the same $Cu_2(BPDC)_2DABCO$ film before and after azobenzene infiltration.
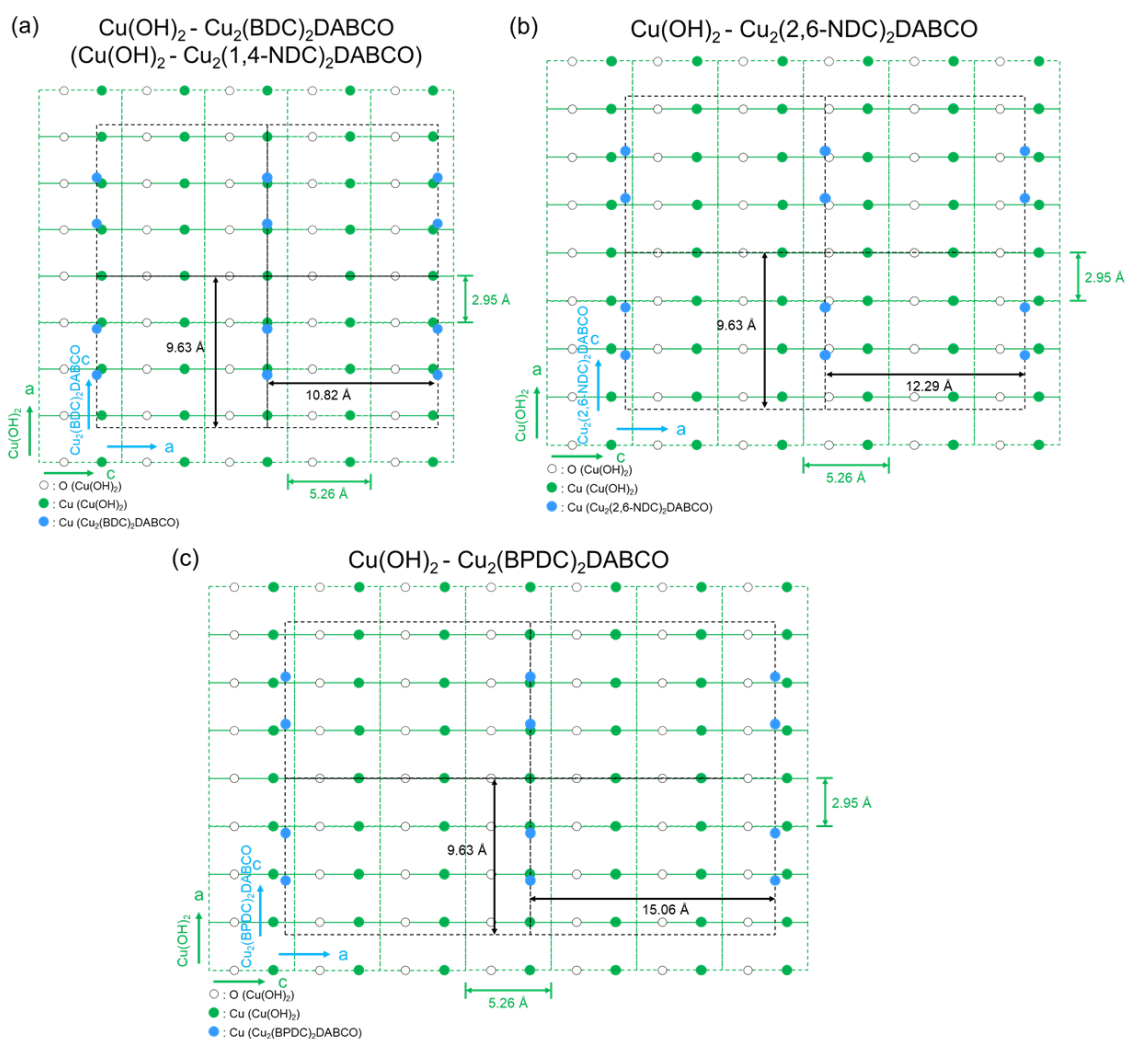
**Figure S2.** Schematic illustration showing crystal lattices of $Cu(OH)_2$ and $Cu_2(Linker)_2DABCO$ from *a-c* and *c-a* projections, respectively. This illustration corresponds to crystal structure on the surface of $Cu(OH)_2$ nanobelts. Cu positions are highlighted by different colors for both crystals (green for $Cu(OH)_2$ and blue for $Cu_2(Linker)_2DABCO$). These values indicate that $Cu(OH)_2$ and $Cu_2(Linker)_2DABCO$ MOFs provide lattice matching conditions for heteroepitaxial growth; lattice mismatches of the $Cu(OH)_2$-$Cu_2(BDC)_2DABCO$ ($Cu_2(1,4-NDC)_2DABCO$), $Cu(OH)_2$-$Cu_2(2,6-NDC)_2DABCO$, and $Cu(OH)_2$-$Cu_2(BPDC)_2DABCO$ systems are 2.85%, 2.74%, and 4.56%, respectively, which were calculated between the lattice constant along the *a* axis of $Cu_2(Linker)_2DABCO$ and the lattice constant multiplied by 2 or 3 along the *c* axis of $Cu(OH)_2$.
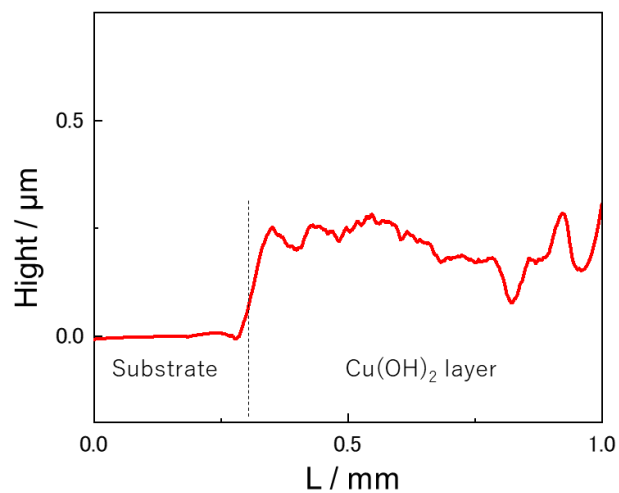
**Figure S3.** Surface roughness profile of an initial $Cu(OH)_2$ layer measured by a stylus profilometer. Thickness of the $Cu(OH)_2$ layer was ca. 220 nm.
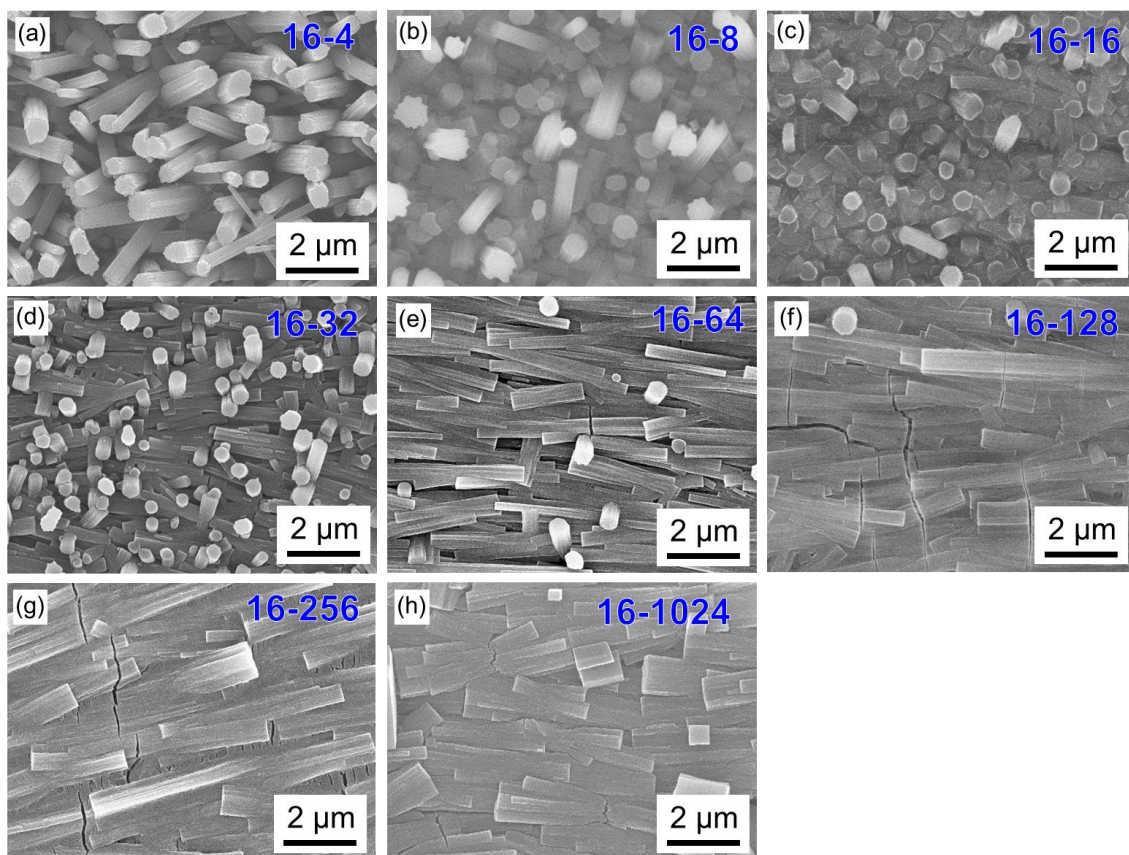


**Figure S4.** SEM images of $Cu_2$(1,4-NDC)$_2$DABCO films synthesized at varied concentrations of 1,4-$H_2$NDC and DABCO; x-y indicate concentration of 1,4-$H_2$NDC and DABCO (mM), respectively.
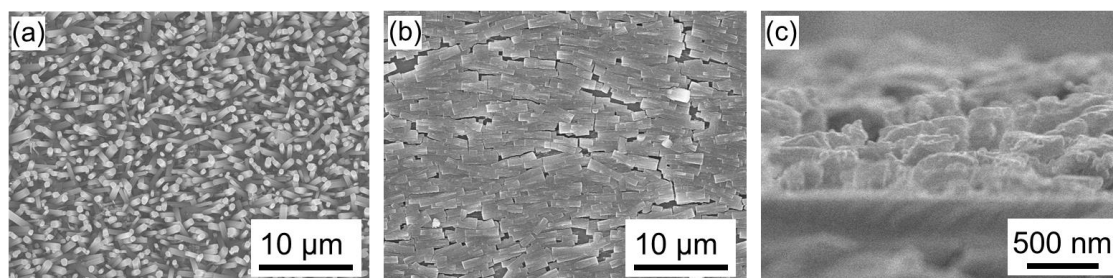
**Figure S5.** Low-magnification SEM images of $Cu_2(1,4\text{-}NDC)_2DABCO$ film synthesized at 16 mM of 1,4-$H_2NDC$ and 4 mM of DABCO (a), and 16 mM of 1,4-$H_2NDC$ and 1024 mM of DABCO (b). Cross-section SEM image of $Cu_2(1,4\text{-}NDC)_2DABCO$ film synthesized at 16 mM of 1,4-$H_2NDC$ and 1024 mM of DABCO along the crystal *a-b* plane.
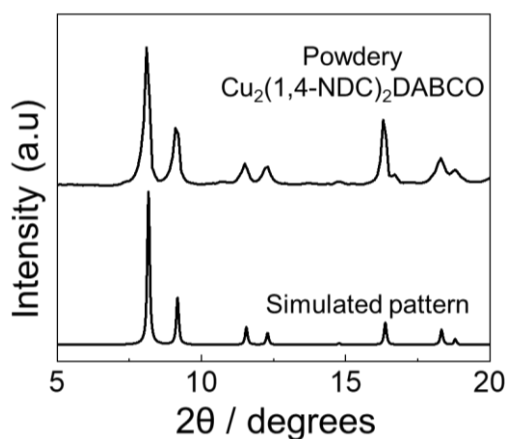


**Figure S6.** XRD pattern of powdery $Cu_2(1,4\text{-}NDC)_2DABCO$. The powdery $Cu_2(1,4\text{-}NDC)_2DABCO$ was synthesized by a homogeneous reaction of $Cu(OH)_2$ nanobelt dispersion with 1,4-$H_2NDC$ and DABCO in methanol at 70 °C for 3 days. The morphology and XRD pattern of the $Cu_2(1,4\text{-}NDC)_2DABCO$ are consistent with those reported so far (e.g., *Angew. Chem. Int. Ed.* **48**, 4739–4743 (2009) and *Angew. Chem. Int. Ed.* **48**, 1766–70 (2009).).
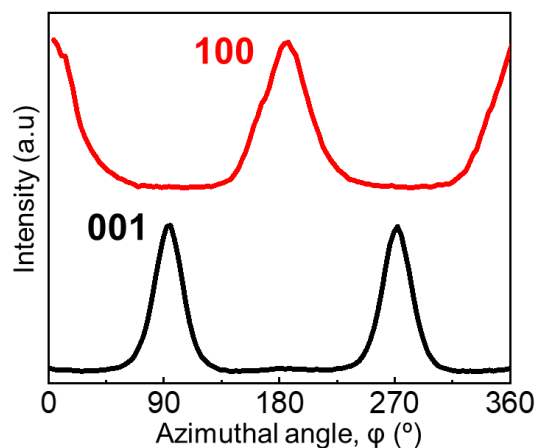
**Figure S7.** Azimuthal angle dependence of intensity profiles of the (100) and (001) reflection of Cu$_2$(1,4-NDC)$_2$DABCO synthesized at the epitaxial growth condition. X-ray incident angle is parallel to longitudinal direction (*a* axis) of Cu(OH)$_2$ nanobelts at $\varphi = 0°$.
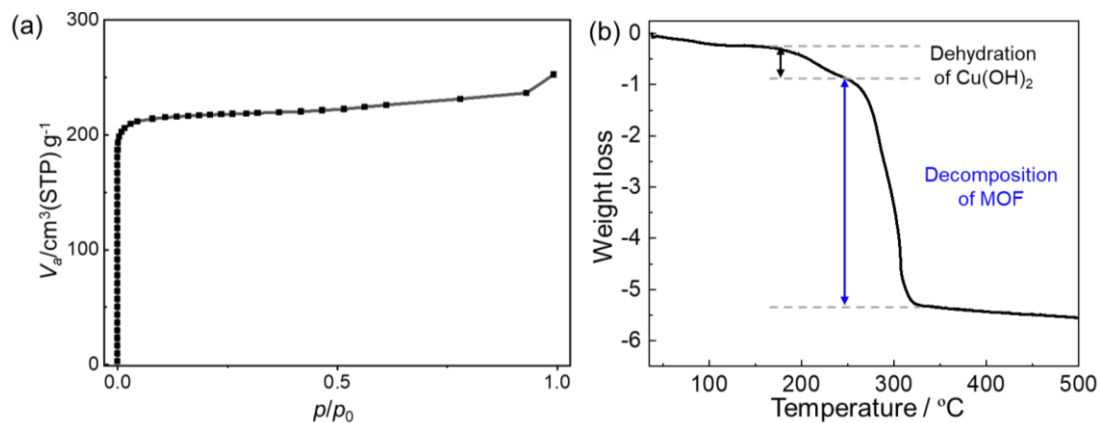


**Figure S8.** (a) N$_2$ gas isotherm and (b) thermogravimetric (TG) curve of Cu$_2$(1,4-NDC)$_2$(DABCO) synthesized with epitaxial growth condition. The 77K N$_2$ gas adsorption analysis was conducted for 66.8 mg of Cu$_2$(1,4-NDC)$_2$(DABCO). The BET surface area is estimated as 984.29 m$^2$/g. The sample weight was corrected with the TG result, which indicates the weight fraction of Cu$_2$(1,4-NDC)$_2$(DABCO) in the MOF/Cu(OH)$_2$ composite as 88.9 %.
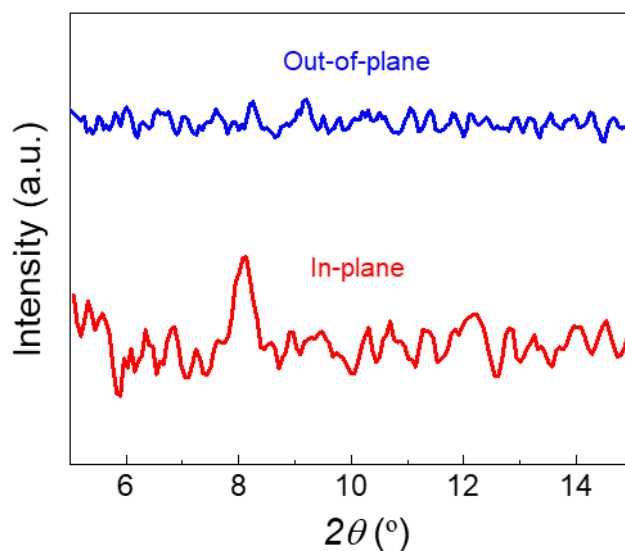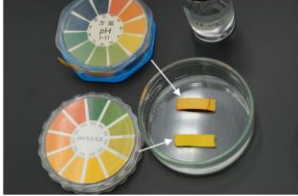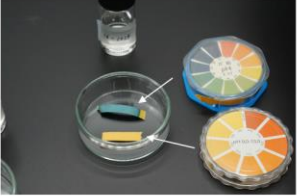
**Figure S9.** Out-of-plane and in-plane XRD patterns of the $Cu_2(1,4\text{-NDC})_2DABCO$ film synthesized at 16 mM of $1,4\text{-H}_2NDC$ and 4 mM of DABCO for 3 min. An diffraction signal is only observed at $2\theta \sim 8.2°$ in the in-plane XRD measurement, suggesting the formation of two-dimensional square lattices composed of Cu paddle-wheel unites linked by 1,4-NDC linkers with the basal face of the crystal parallel to the substrate.
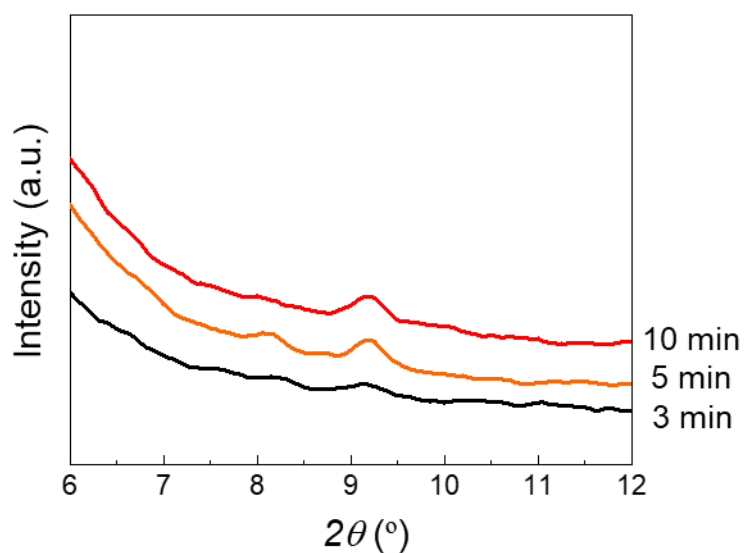


**Figure S10.** Out-of-plane XRD patterns of the $Cu_2(1,4\text{-NDC})_2DABCO$ film synthesized at 16 mM of $1,4\text{-H}_2NDC$ and 4 mM of DABCO for 3, 5, and 10 min.
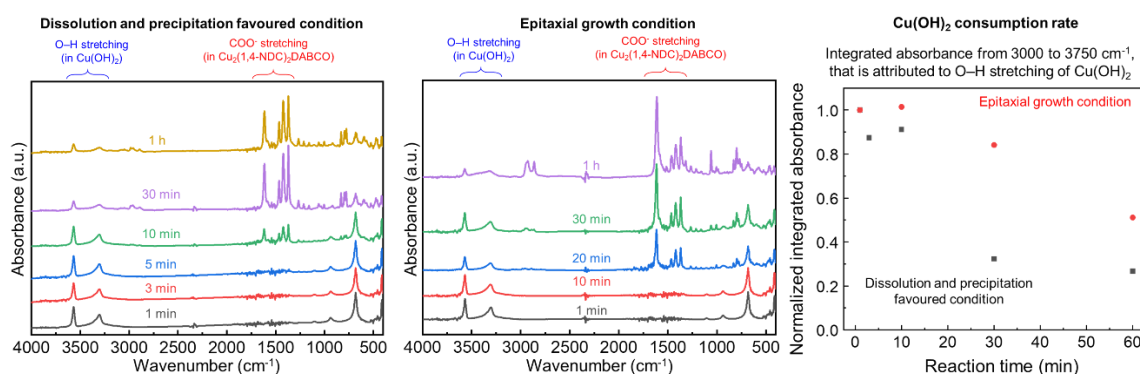
**Figure S11.** FT-IR spectra of $Cu_2$(1,4-NDC)$_2$DABCO synthesized at the dissolution and precipitation favoured condition and epitaxial growth condition with varied reaction time. Under the dissolution and precipitation favoured condition, the formation of the MOF was detected at the reaction time of 10 min. While, under the epitaxial growth condition, the formation of the MOF was detected at the reaction time of 20 min. The $Cu(OH)_2$ consumption under the dissolution and precipitation favoured condition was faster than that under the epitaxial growth condition.



**Figure S12.** The reaction solution pH for linker-rich and DABCO-rich conditions before and after reaction. The solution pH was investigated by a pH indicator paper. pH of the solution for the linker-rich condition was 4.0, and pH of the solution for the DABCO-rich condition and was 9.0. Under both conditions, the solution pH did not alter after reaction.
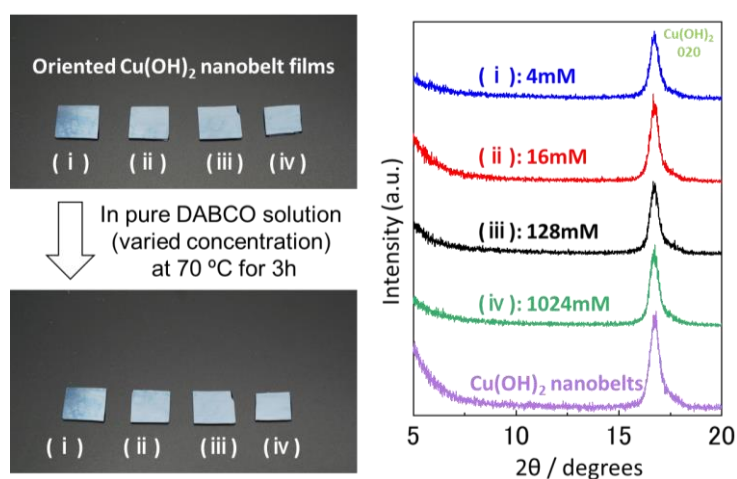
**Figure S13.** A control experiment showing the reactivity of $Cu(OH)_2$ in DABCO solutions (in methanol) at 70 ºC for 3h. XRD measurement confirms $Cu(OH)_2$ does not react in DABCO solution.
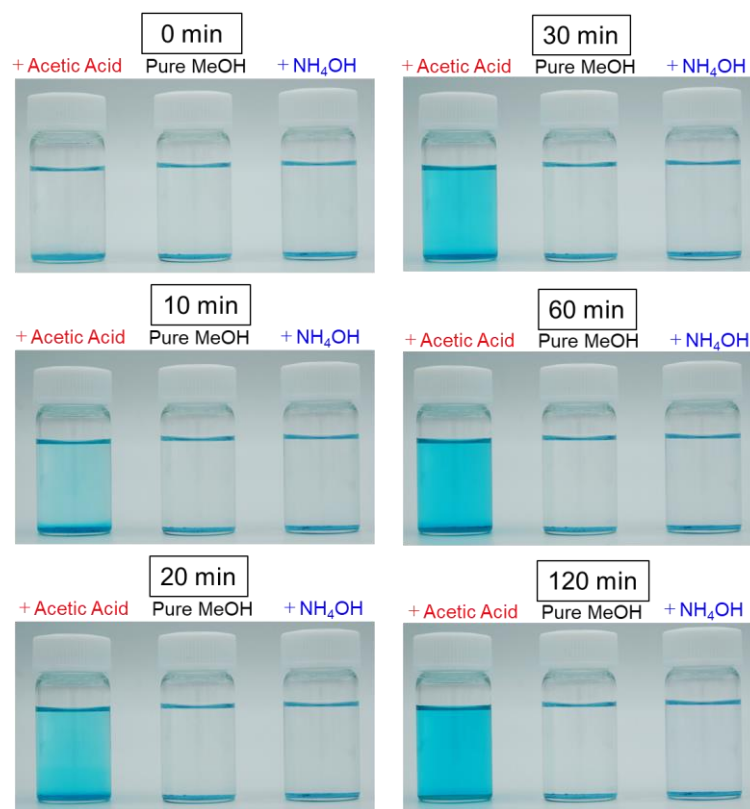


**Figure S14.** Dissolution test of $Cu(OH)_2$ nanobelts (10 mg) in 10 mL of pure methanol and methanol containing acetic acid (50 mM, 28.6 μL of 99.7% acetic acid) or $NH_4OH$ (50 mM, 30.4 μL of 28% $NH_3$ aq.). The appearance of blue color indicates the presence of $Cu^{2+}$ by the dissolution of $Cu(OH)_2$ nanobelts.

**1,4-H$_2$NDC 4 mM, DABCO 32 mM**

**+ Acetic acid 10 mM**

**+ Acetic acid 50 mM**

(a) 1 μm

(b) 1 μm

(c) 1 μm

**1,4-H$_2$NDC 16 mM, DABCO 4 mM**

**+ NH$_4$OH 15 mM**

**+ NH$_4$OH 25 mM**

(e) 1 μm

(f) 1 μm

(g) 1 μm
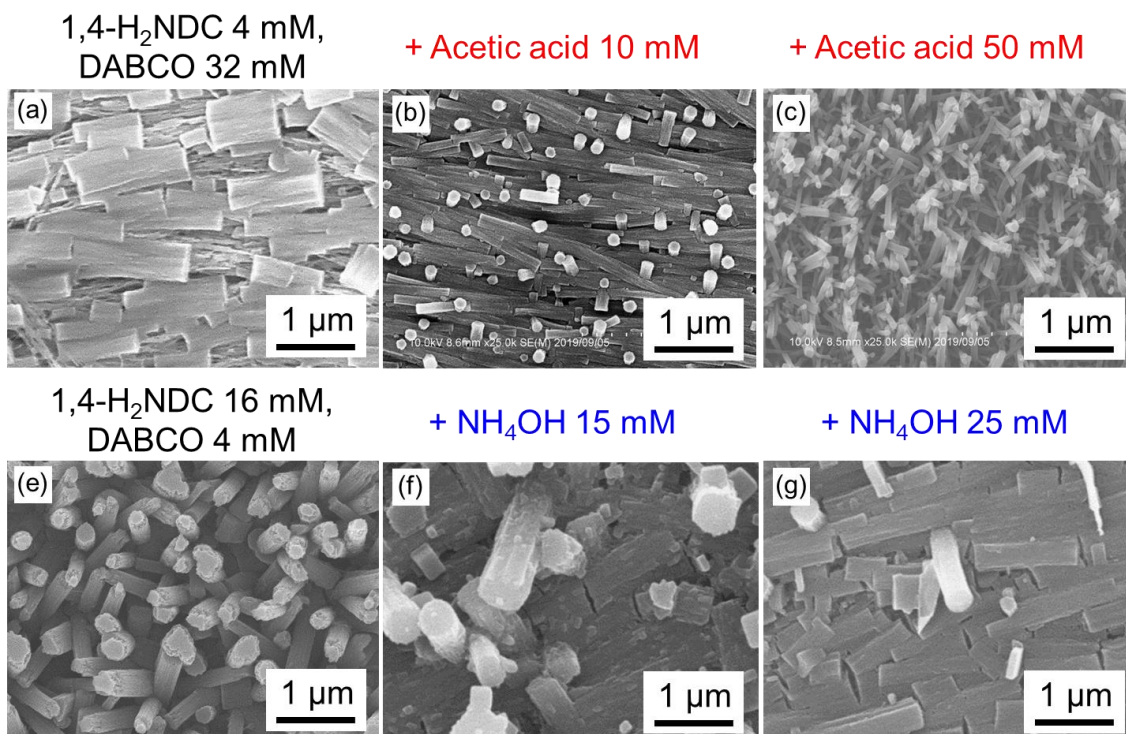
**Figure S15.** SEM images of Cu$_2$(1,4-NDC)$_2$DABCO films synthesized at fixed concentration of 1,4-H$_2$NDC and DABCO with an addition of acid (acetic acid) or base (NH$_4$OH). The reaction solution for the addition of acid was prepared by adding 5.7 μL (10 mM) or 28.6 μL (50 mM) of 99.7% acetic acid to 10 mL methanol containing 1,4-H$_2$NDC (4 mM) and DABCO (32 mM). The reaction solution for the addition of base was prepared by adding 9.1 μL (15 mM) or 15.2 μL (25 mM) of 28% NH$_3$ aqueous solution to 10 mL methanol containing 1,4-H$_2$NDC (16 mM) and DABCO (4 mM).
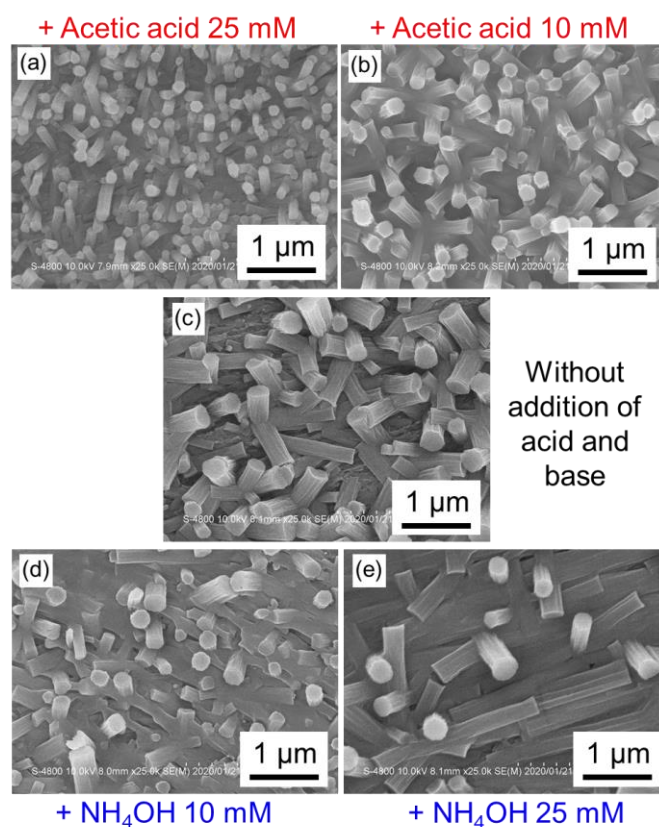
**Figure S16.** SEM images of Cu$_2$(1,4-NDC)$_2$DABCO films synthesized at fixed concentration of 1,4-H$_2$NDC (16 mM) and DABCO (32 mM) with addition of acid (acetic acid) or base (NH$_4$OH). The reaction solution for the addition of acid was prepared by adding 5.7 μL (10 mM) or 14.3 μL (25 mM) of 99.7% acetic acid to 10 mL methanol containing 1,4-H$_2$NDC and DABCO. The reaction solution for the addition of base was prepared by adding 6.1 μL (10 mM) or 15.2 μL (25 mM) of 28% NH$_3$ aqueous solution to 10 mL methanol containing 1,4-H$_2$NDC and DABCO. Elongated brick shape Cu$_2$(1,4-NDC)$_2$DABCO crystals both perpendicular and parallel to the substrate were observed without addition of acid and base. The MOF crystals perpendicular to the substrate dominated with the addition of acid. In contract, the addition of base resulted in the MOF crystals parallel to the substrate. This result clearly shows that the orientation of the MOF films is controllable by simply changing the solution acidity and basicity.
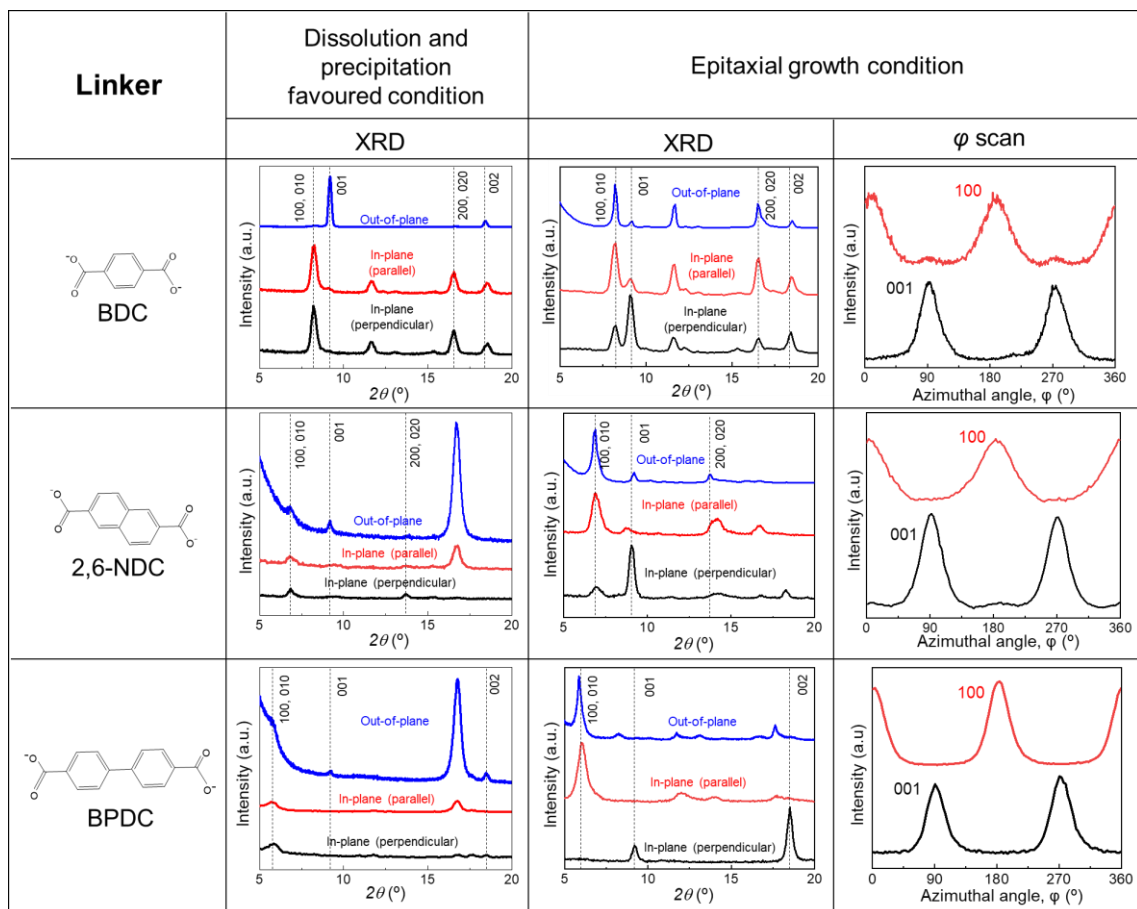
**Figure S17.** Summary of XRD patterns and azimuthal angle dependence of intensity profiles of Cu$_2$(Linker)$_2$DABCO (Linker=BDC, 2,6-NDC, and BPDC) film synthesized under dissolution and precipitation favoured condition and epitaxial growth condition. Three setups for the XRD investigations were used; out-of-plane (blue line), in-plane (red and black line, X-ray incident angle is parallel and perpendicular to longitudinal direction of nanobelts at $\varphi = 0°$). Azimuthal angle dependences of intensity profiles were collected for the (100) and (001) reflection of Cu$_2$(Linker)$_2$DABCO synthesized at epitaxial growth condition. X-ray incident angle is parallel to longitudinal direction (*a* axis) of Cu(OH)$_2$ nanobelts at $\varphi = 0°$. The XRD investigations and azimuthal angle dependence of intensity profiles clearly show that dissolution and precipitation favoured condition resulted in the fabrication of Cu$_2$(Linker)$_2$DABCO films with the 1D nanochannels (*c* axis) perpendicular to substrates, and Cu$_2$(Linker)$_2$DABCO films with the 1D nanochannels (*c* axis) parallel to substrates in the same direction are fabricated under the epitaxial growth condition.
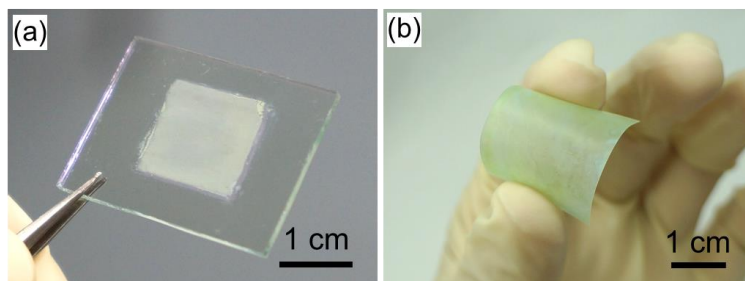
**Figure S18.** Large-scale fabrication ($15 \times 15$ mm$^2$) of aligned Cu$_2$(1,4-NDC)$_2$DABCO films on a conductive ITO substrate (**a**) and a poly ethylene terephthalate (PET) film (b).
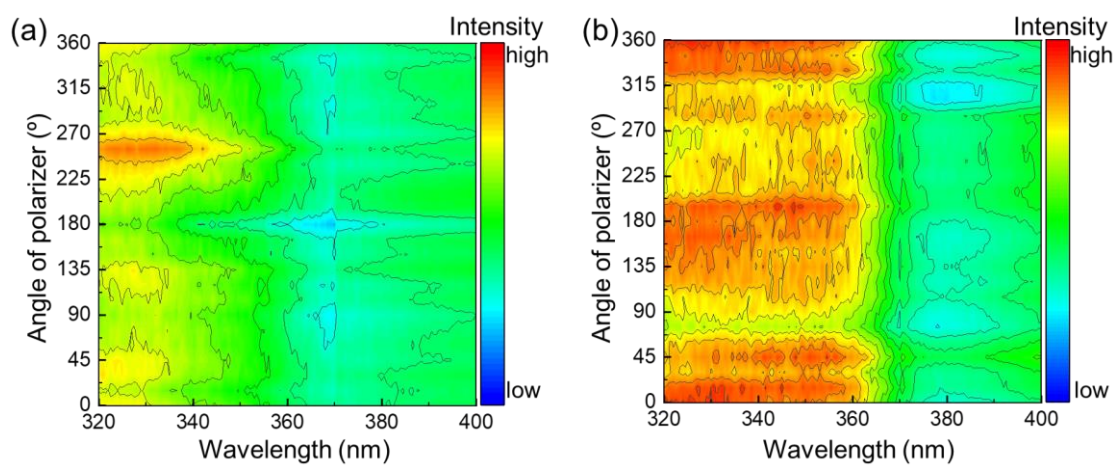


**Figure S19.** 3D intensity plots of polarization-dependent UV/Vis difference absorption spectra (a) before and (b) after AZB inclusion into the Cu$_2$(BPDC)$_2$DABCO oriented film.
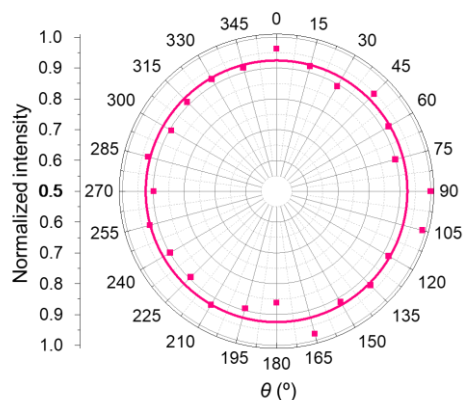
**Figure S20.** Angular dependence of a polarizer in integrated absorption from 330 to 380 nm for a randomly oriented Cu$_2$(BPDC)$_2$DABCO film including AZB. The randomly oriented Cu$_2$(BPDC)$_2$DABCO film was synthesized from randomly oriented Cu(OH)$_2$ nanobelts film at the same condition for the Cu$_2$(BPDC)$_2$DABCO oriented film.
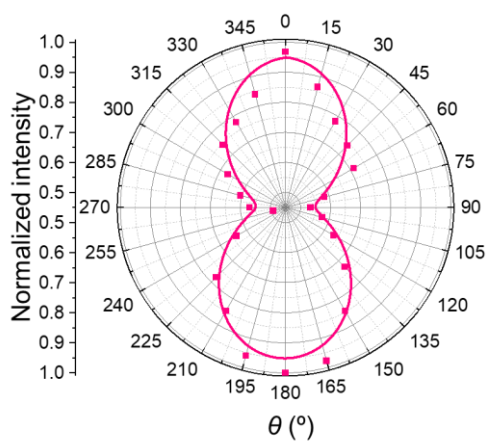


**Figure S21.** Angular dependence of a polarizer in integrated absorption from 330 to 380 nm for the AZB-included Cu$_2$(BPDC)$_2$DABCO oriented film after repeated *trans–cis* isomerization.

14